



GSV-SRTS: a heterogeneous landscape soil-canopy reflectance model over sloping terrain with an extended GSV and stochastic radiative transfer theory

Siqi Li¹, Guyue Hu^{1,2}, Shaoda Li¹, Ronghao Yang¹, Junxiang Tan¹, Chenghao Liu¹, and Jinhu Bian^{2,3}

¹College of Earth and Planetary Sciences, Chengdu University of Technology, Chengdu 610059, China

²Wanglang Mountain Remote Sensing Observation and Research Station of Sichuan Province, Mianyang 621000, China

³Institute of Mountain Hazards and Environment, Chinese Academy of Sciences, Chengdu 610213, China

Correspondence: Guyue Hu (hugy@cdut.edu.cn)

Received: 19 October 2025 – Discussion started: 4 January 2026

Revised: 13 April 2026 – Accepted: 19 April 2026 – Published: 30 April 2026

Abstract. Accurately modelling radiation interactions within canopy layers and soil backgrounds is crucial for biophysical variables retrieval across regional or global scales. However, terrain relief introduces significant uncertainties in modeling CR by modulating solar and viewing geometry and exacerbating landscape heterogeneity. Traditional CR models, designed primarily for flat and homogeneous landscapes, often inadequately represent these complex interactions. In this study, we present a canopy reflectance model suitable for heterogeneous structures on sloping terrain. By extending the stochastic radiative transfer theory from flat terrain to sloping terrain and integrating the soil General Spectral Vector, the GSV-SRTS model was introduced. This enables accurate prediction of soil-canopy radiative transfer within subpixel 3D heterogeneous mountain landscapes. The proposed GSV-SRTS model was evaluated against the Discrete Anisotropic Radiative Transfer (DART) model, compared with typical mountain canopy reflectance models, and validated against remote sensing observations at varying spatial resolutions. The results showed that the GSV-SRTS model achieves good accuracy in the comparisons with DART ($R^2 = 0.9136$ (0.9052) and root-mean-square errors (RMSE) = 0.0246 (0.0216) in the red (NIR (Near-Infrared)) band) and performs well in real mountainous areas, particularly with high spatial resolution remote sensing observations ($R^2 = 0.9078$ (0.9143) and RMSE = 0.0201 (0.0212)). Furthermore, the GSV-SRTS model effectively captures the impacts of canopy structure and terrain factors on bidirectional reflectance. This underscores the GSV-SRTS model as

a reliable physical tool for simulating radiation regimes over sloping terrain, with the potential to enhance the accuracy of biophysical variable retrieval from remote sensing observations.

1 Introduction

Canopy reflectance (CR) models simulate radiative transfer within vegetation-soil systems to link biophysical parameters with remote sensing data (Widlowski et al., 2013). Accurate simulation of these processes is fundamental for interpreting remote sensing observations and retrieving biophysical variables across scales (Verrelst et al., 2015). However, to manage the inherent heterogeneity of reality, CR models necessarily use abstractions and simplifications (Yin et al., 2017), which consequently limits their ability to characterize fine-scale landscape details.

In addition, topography presents challenges in CR modeling, as terrain relief modifies illumination and viewing geometry, leading to variations in radiance through surface anisotropic reflectance (Sandmeier and Itten, 1997), and significantly affecting the gap probability of canopy layers, which alters radiation contributions from both the canopy and soil background in solar and viewing directions (Wen et al., 2018). Therefore, the heterogeneous landscapes and sloping terrain are the primary sources of uncertainty in CR modeling (Yin et al., 2017).

In recent decades, a variety of models for canopy reflectance on sloping terrain have been developed. Schaaf et al. (1994) introduced the geometric-optical (GO) and mutual shadowing models to sloping terrain (GOMST) by applying the coordinate rotation (Schaaf et al., 1994). Combal et al. (2000) expanded the Ross model (Ross, 2012) to account for sloping terrain while maintaining geotropic vegetation growth (Combal et al., 2000). Verhoef and Bach (2007, 2012) developed a framework that integrated radiative transfer (RT) processes within a soil-leaf-canopy (SLC) medium and later extended this model to sloping terrain (SLCT) (Verhoef and Bach, 2007, 2012). However, these CR models overlooked the impact of the heterogeneity of canopy structure and soil properties and assumes that they are uniformly distributed in pixels.

The characterization of canopy heterogeneity structure is a crucial aspect in remote sensing studies. The geometric-optical model over sloping terrain (GOST) has been utilized to represent the realistic 3D structure of canopy (Fan et al., 2014). However, the computational complexity of GOST has limited its performance in parameter retrieval. The canopy reflectance model suitable for both continuous and discontinuous canopies over sloping terrain (BOST) was developed (Hu and Li, 2022). However, the internal canopy structure was based on the assumption of turbid media which inherited from the SLC model. To overcome these limitations, the Stochastic Radiative Transfer (SRT) theory was drawn into canopy RT modeling, which simulates the random scattering and absorption of photons as they interact with various canopy elements, allowing for a more realistic representation of the three-dimensional (3D) structure of vegetation (Shabanov et al., 2000). This makes SRT a suitable approach for complex and heterogeneous scenarios (Shabanov et al., 2007). Zeng et al. developed a RT model specifically designed for patchy landscapes based on SRT theory (Zeng et al., 2020), which considered landscape heterogeneity by integrating stochastic processes to simulate radiation interactions within fragmented vegetation canopies, addressing variability in canopy structure and spatial distribution. Yan et al. applied the SRT model to heterogeneous discrete canopies (Yan et al., 2021), achieving an optimal balance between accuracy and efficiency in modeling radiation regimes of discontinuous canopies. Li et al. (2020) expanded SRT to simulate BRDF in forests with within-crown heterogeneity, parameterizing vertical and horizontal foliage distributions to enable simulations of complex canopy structures while maintaining theoretical consistency with 3D radiative transfer (Li et al., 2020). While SRT models have proven effective in characterizing RT within heterogeneous canopies, their performance in mountainous regions is limited by the neglect of terrain effects. Extending the SRT theory to sloping terrain could enhance the characterization of RT within mountain vegetation, providing a more comprehensive understanding of canopy heterogeneity in such challenging environments.

In terms of quantitative impacts on CR modelling, soil reflectance is a key factor in the accurate modeling of canopy reflectance, especially in areas with sparse vegetation. Under canopies with a low leaf area index ($LAI < 2$), soil reflectance can contribute significantly to the total canopy reflectance, particularly in the near-infrared (NIR) region (Jacquemoud et al., 2009). Neglecting soil reflectance in canopy reflectance (CR) models can lead to errors of 10%–30% in reflectance estimates (Baret et al., 1993). Research has shown that incorporating precise soil reflectance data into radiative transfer (RT) models can improve simulation accuracy by 5%–15% (Jacquemoud et al., 2009). To better capture the heterogeneity of soil properties across landscapes, empirical methods are commonly used to model soil spectral reflectance. Jiang and Fang (2019) developed the General Spectral Vector (GSV) model, which combines site-specific observational data with soil databases to accurately simulate soil reflectance spectra (Jiang and Fang, 2019). The GSV model has been found to outperform traditional wet chemical methods in soil monitoring (Nocita et al., 2015) and has demonstrated effectiveness in predicting soil properties even in vegetated areas (Pinheiro et al., 2017).

To address the terrain effects and consider both the heterogeneity of canopy structure and soil properties, a new soil-canopy reflectance model known as GSV-SRTS was developed in this study specifically for sloping heterogeneous landscapes by expanding on the GSV and SRT theory. The canopy gap probability modulated by terrain factors, geotropic growth of vegetation, and terrain-induced variations in illumination and viewing geometry were taken into account. GSV-SRTS can offer a realistic representation of radiation propagation within soil-canopy objects over sloping terrains, serving as a theoretical tool for forward canopy reflectance modeling over sloping terrains with heterogeneous vegetation structures. This model has the potential to be used to accurately retrieve biophysical parameters related to vegetation. To further explore how terrain and vegetation characteristics impact canopy and soil reflectance, the GSV-SRTS model was used to analyse the effects of different terrain factors and canopy gap probabilities on model performance.

The following sections will provide a detailed overview of the article. In Sect. 2, we will delve into the development of the GSV-SRTS model. Section 3 will outline the evaluation strategy, including the DART configuration and validation using actual remote sensing images. Moving on to Sect. 4, we will present the results of the validation and performance assessment of the model. Sections 5 and 6 will then offer a discussion of the findings and conclude with final remarks.

2 Methods

The accurate simulation of canopy reflectance (CR) over sloping terrain requires a physically consistent coupling of the soil background contribution with the radiative trans-

fer within the vegetation canopy. The soil background is not merely a static lower boundary but a spectrally variable source of reflected radiation that interacts multiple times with the canopy (e.g., through ground-canopy-ground scattering). In heterogeneous mountainous landscapes, both the soil spectral properties and the canopy architecture vary spatially. Therefore, an integrated framework is necessary. In this study, we couple a General Spectral Vector (GSV) model for the soil background with a Stochastic Radiative Transfer (SRT) model for the canopy. The GSV model efficiently represents the high-dimensional spectral variability of soils, providing the lower boundary condition. The SRTS model, operating within a local slope coordinate system, simulates the absorption and scattering of radiation within a 3D heterogeneous canopy. The coupling occurs physically at the soil-canopy interface: the anisotropic reflectance field from the GSV soil model serves as the upwelling boundary condition for the SRT equation, while the SRT-computed transmission and multiple scattering determine the irradiance incident upon the soil. This bidirectional coupling ensures that the combined GSV-SRTS model captures the integrated effect of variable soils and complex canopies under terrain-modified illumination.

2.1 General Framework of the GSV-SRTS Model

The GSV-SRTS model is a sophisticated theoretical framework designed to address the intricate nature of radiation transfer processes within the layers of a canopy. By expanding upon the traditional radiation transfer equation to include the soil GSV and integrating topographic elements, this model offers a more precise depiction of the inherent variations present in canopy-soil systems. One key feature of the GSV-SRTS model is its utilization of a local slope coordinate system for all internal calculations, ensuring a geometrically accurate representation of how light interacts within a rugged mountainous terrain. To illustrate the application of the GSV-SRTS model, this study presents a 3D discontinuous canopy made up of identical trees situated within the layer defined as $0 < z < H$ in the coordinate system (Fig. 1). The number of trees housed within a pixel is determined randomly using the Poisson distribution (Huang et al., 2008). From a stochastic view, the 3D canopy structure is conceptualized as a spatial stochastic process, symbolized by an indicator function denoted as $\chi(x, y, z)$. This function yields a value of 1 if the specific point (x, y, z) falls under vegetation cover, and 0 if it does not.

2.2 Stochastic radiative transfer equation in sloping terrains

The adoption of a local slope coordinate system (x', y', z') , aligned with the inclined ground surface, is fundamentally necessary to render the radiative transfer problem tractable over slopes. In the conventional horizontal coordinate sys-

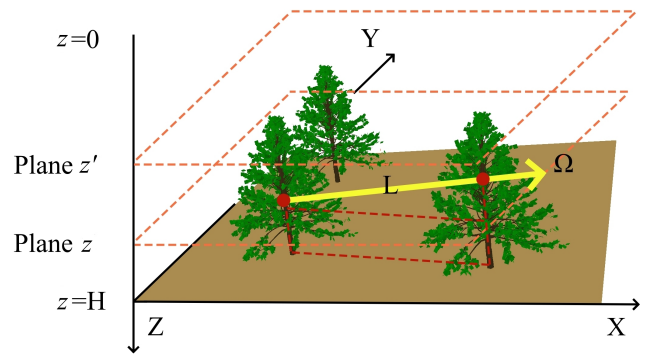


Figure 1. A typical discontinuous vegetation canopy and the coordinate system used for the stochastic RT equation. The planes $z = 0$ and $z = H$ represent the top and bottom boundaries of the vegetation canopy, respectively. A specific point within the vegetation canopy, located on the plane z , moves upward along the unit vector Ω , covering a distance L until it reaches the plane z' .

tem, a sloping ground surface presents a moving, tilted boundary condition that vastly complicates the formulation of the extinction coefficient and the boundary conditions for the radiative transfer equation (RTE). By transforming to a coordinate system where the z' axis is normal to the local slope, the ground surface is redefined as a flat plane ($z' = 0$). This crucial simplification allows the use of a standard volumetric formulation for canopy extinction and enables the application of the stochastic approach for gap probability calculation on this effectively “level” domain. Consequently, all canopy structural statistics and radiative transfer calculations are performed relative to this local frame, and the effects of terrain are encapsulated in the modified solar and viewing direction vectors within this frame, as defined in Eqs. (1)–(3). For any given global direction Ω , its corresponding local sun zenith angle $\cos \theta_s$ and local view zenith angle $\cos \theta_v$ are calculated as (Gu and Gillespie, 1998):

$$\cos \theta_{s(v)} = \cos \theta_g \cos \theta'_{s(v)} + \sin \theta_g \sin \theta'_{s(v)} \cos \varphi_{sg(vg)} \quad (1)$$

where θ_g and φ_g represent the slope and aspect, respectively. φ_{sg} is the relative azimuth angle between the sun and the sloping background; and φ_{vg} is the relative azimuth angle between the viewer and the sloping background. All subsequent RT computations inside the canopy are performed using these local angles, ensuring that all physical interactions are relative to the actual inclined surface.

The Stochastic Radiative Transfer Equations (SRTE) are obtained through horizontal averaging of the 3D RT process, thereby integrating the influence of canopy structure. Solving these equations (Eqs. 2 and 3) necessitates determining the mean radiation intensities for both the entire scene, $\bar{I}(z, \Omega)$, and the vegetation-covered area within a pixel, $U(z, \Omega)$, at depth z in direction Ω , which are defined as (Vainikko, 1973; Shabanov et al., 2000):

$$\begin{aligned} \mu \frac{\partial \bar{I}(z, \Omega)}{\partial z} = & -\sigma'(\Omega)\bar{I}(z, \Omega) \\ & + \frac{\sigma_s}{4\pi} \int_{4\pi} \bar{I}(z, \Omega')\sigma'_s(\Omega', \Omega)d\Omega' \\ & + F_0(z, \Omega) + F_H(z, \Omega) \end{aligned} \quad (2)$$

$$\begin{aligned} \mu \frac{\partial U(z, \Omega)}{\partial z} = & -\sigma'(\Omega)U(z, \Omega) \\ & + \frac{\sigma_s}{4\pi} \int_{4\pi} U(z, \Omega')\sigma'_s(\Omega', \Omega)d\Omega' \\ & + Q_0(z, \Omega) + Q_H(z, \Omega) \end{aligned} \quad (3)$$

where $\mu = \cos\theta_v$, and θ is the local view zenith angle. Ω indicates the direction of incoming direct light, and Ω' indicates the viewing direction. $F_0(z, \Omega)$ and $F_H(z, \Omega)$ in Eq. (2) represent the diffuse and direct radiation entering through the upper and lower boundaries. $Q_0(z, \Omega)$ and $Q_H(z, \Omega)$ in Eq. (3) refer to the mean diffuse and direct radiation that penetrate the upper and lower canopy boundaries and subsequently experience scattering in the heterogeneous medium. $\sigma'(\Omega)$ is the extinction coefficient. The extinction coefficient is geometrically corrected to account for local slope-induced projection effects. This correction reduces effective extinction when illumination or viewing directions are highly oblique relative to the local normal, ensuring the local radiative balance remains consistent with the actual slope geometry, which is shown as follows (Mousivand et al., 2015):

$$\sigma'(\Omega) = \sigma(\Omega)\sqrt{\max(0, \mu'_s)\max(0, \mu'_v)} \quad (4)$$

The terrain-induced azimuthal dependence of scattering is characterized by a topographic modulation function (Sandmeier and Itten, 1997). The modulation function, which depends on the local slope angle and the directions relative to the slope normal, physically approximates the effect of this truncated geometry on the scattering process. It adjusts the standard volumetric scattering phase function to better represent the anisotropic scattering behavior in the vicinity of the sloping ground boundary, where the hemispherical distribution of scatterers is asymmetrically constrained. It is described as follows:

$$C_{\text{topo}}(\phi_v) = \sin\theta_g \cos\phi_{vg} \mu'_s \mu'_v \quad (5)$$

which enhances scattering in the downslope direction and weakens it in the upslope direction. The scattering kernel $\sigma_s(\Omega', \Omega)$ in Eqs. (2) and (3) is adjusted by the slope-induced azimuthal modulation function:

$$\sigma'_s(\Omega', \Omega) = \sigma_s(\Omega', \Omega) [1 + C_{\text{topo}}(\phi_v)] \quad (6)$$

where $\sigma_s(\Omega', \Omega)$ is the original differential scattering coefficient (using a Henyey–Greenstein phase function).

The average horizontal intensity across over vegetated area $U(z, \Omega)$ or the entire horizontal plane $\bar{I}(z, \Omega)$ comprise two

components: the direct and the diffuse parts of the incoming irradiance, which can be given as follows (Shabanov et al., 2000):

$$\begin{aligned} U(z, \Omega) &= U_{\text{dir}}\delta(\Omega' - \Omega) + U_{\text{dif}}(z, \Omega) \\ \bar{I}(z, \Omega) &= f_{\text{dir}}I_{\text{dir}}\delta(\Omega' - \Omega) + I_{\text{dif}}(z, \Omega) \end{aligned} \quad (7)$$

where f_{dir} is the fraction of incident direct radiation on the upper boundary; $\delta(\Omega' - \Omega)$ is Dirac's delta function (Dirac, 1981), which approaches infinity when the polar angle in direction Ω matches the direction of direct solar radiation Ω , and zero otherwise; $U_{\text{dir}}(z)$ ($I_{\text{dir}}(z)$) and $U_{\text{dif}}(z, \Omega)$ ($I_{\text{dif}}(z, \Omega)$) represent the direct component and the diffuse component over the vegetation-occupied area (or the entire scene area), respectively, which is described in Eq. (7). The boundary conditions for the entire scene are simplified as follows (Shabanov et al., 2000; Bird and Hulstrom, 1981).

$$\begin{aligned} \bar{I}_0(z, \Omega) &= F_{\text{dir}}(\Omega_0)\delta(\Omega - \Omega_0) + d_0(z, \Omega), u < 0 \\ I_H(z, \Omega) &= \frac{R(\Omega, \Omega')}{\pi \int_{2\pi^+} R(\Omega, \Omega') \cos\theta_v d\Omega} + d_H(z, \Omega), u > 0 \end{aligned} \quad (8)$$

$$F_{\text{dir}} = S_0 \cos\theta_s T \quad (9)$$

$$\rho_{\text{soil}} = \frac{1}{\pi} \int_{2\pi^+} R(\Omega, \Omega') \cos\theta_v d\Omega \quad (10)$$

where $\delta(\Omega - \Omega_0)$ is the Dirac's delta function, which enables precise estimation of the solar radiation. $F_{\text{dir}}(\Omega_0)$ represents the intensity of direct radiation incident on the upper boundary. S_0 is the solar constant, and T is the atmospheric transmittance. $d_0(z, \Omega)$ denotes the diffuse radiation intensity from the upper boundary, while $d_H(z, \Omega)$ represents the intensity entering the canopy through the lower boundary. These two parameters can be calculated using the Second Simulation of the Satellite Signal in the Solar Spectrum (6S) model (Roujean et al., 1992). The 6S model calculates $d_0(z, \Omega)$ as atmospheric diffuse skylight via RTE accounting for Rayleigh and aerosol scattering and $d_H(z, \Omega)$ by integrating surface/canopy scattering effects on transmitted radiation. $R(\Omega, \Omega')$ is the bidirectional soil reflectance factor, the same as $R_{1 \times l}$ in Eq. (20) and ρ_{soil} is the soil hemispherical reflectance. The incoming radiation can be parameterized by two values: the total flux $F_{\text{dir}+\text{dif}}(\Omega_0)$, defined as follows (Shabanov et al., 2000):

$$\begin{aligned} F_{\text{dir}+\text{dif}}(\Omega_0) &= \int_{2\pi^-} \bar{I}_0(z, \Omega) \cos\theta_v d\Omega \\ &= F_{\text{dir}} \cos\theta_v + \int_{2\pi^-} d_0 \cos\theta_v d\Omega \end{aligned} \quad (11)$$

The horizontal average intensity $U(z, \Omega)$ over the vegetation-covered area can be decomposed into the direct ($U_{\text{dir}}(z)$) and diffuse ($U_{\text{dif}}(z)$) components of the incoming solar radiation, defined as follows (Shabanov et al., 2000):

$$\begin{cases} U_{\text{dir}}(z) + \frac{\sigma(\Omega)}{|\cos\theta_v|} \int_0^z K(z, z', \Omega) U_{\text{dir}}(z', \Omega) dz' = 1 \\ \begin{cases} U_{\text{dif}}(z, \Omega) + \frac{\sigma(\Omega)}{|\cos\theta_v|} \int_0^z K(z, z', \Omega) U_{\text{dif}}(z', \Omega) dz' \\ = \frac{1}{|\cos\theta_v|} \int_0^z K(z, z', \Omega) S_{\text{dif}}(z', \Omega) dz' + F_0(z, \Omega), \mu < 0 \\ U_{\text{dif}}(z, \Omega) + \frac{\sigma(\Omega)}{|\cos\theta_v|} \int_z^H K(z, z', \Omega) U_{\text{dif}}(z', \Omega) dz' \\ = \frac{1}{|\cos\theta_v|} \int_z^H K(z, z', \Omega) S_{\text{dif}}(z', \Omega) dz' + F_H(z, \Omega), \mu > 0 \end{cases} \end{cases} \quad (12)$$

$$S_{\text{dif}}(z', \Omega) = \int_{4\pi} \sigma_s(\Omega \rightarrow \Omega') U_{\text{dif}}(z', \Omega') d\Omega' \quad (13)$$

where $S_{\text{dif}}(z', \Omega)$ denotes the spherical integration of scattering. $K(z, z', \Omega)$ is the Conditional Probability Correlation Function (PCF). This core function quantifies the probability of spatial correlation between vegetation elements at depths z and z' along direction Ω , thereby statistically capturing the effect of canopy 3D structure and heterogeneity on the radiation field. The stochastic canopy structure is embedded in the SRTE solution via the PCF, which encodes spatial correlations of vegetation presence derived from $\chi(x, y, z)$. This function directly modulates the integral terms in Eq. (12), ensuring canopy heterogeneity and terrain-slope effects are propagated through radiation intensities. Its mathematical form is shown as follows (Shabanov et al., 2007):

$$q(z, z', \Omega) = \left\langle \frac{1}{S} \iint_S \chi(x, y, z) \chi(x', y', z') \cdot f(\theta_g, \Delta h) dx dy \right\rangle \quad (14)$$

$$f(\theta_g, \Delta h) = \exp\left(-\frac{\Delta h}{H \cdot \tan\theta_g}\right) \quad (15)$$

$$p(z) = \left\langle \frac{1}{S} \iint_S \chi(x, y, z) dx dy \right\rangle \quad (16)$$

$$K(z, z', \Omega) = \frac{q(z, z', \Omega)}{p(z)} = \left\langle \frac{\int_S \chi(x, y, z) \chi(x', y', z') dx dy}{\iint_S \chi(x, y, z) dx dy} \right\rangle \quad (17)$$

where $p(z)$ is the canopy density at canopy depth z , $\chi(x, y, z)$ is the indicator function (1 for vegetation, 0 otherwise). The point (x, y, z) moves travels a distance L in the direction Ω to reach (x', y', z') . The bracket $\langle \cdot \rangle$ denotes the ensemble average over all realizations of $\chi(x, y, z)$ within a finite pixel. Δh is the vertical elevation difference between two points, H is the total vertical height of the vegetation canopy.

2.3 Reflectance factors of the soil background

Soil reflectance properties are important elements that should be carefully formulated in canopy radiative transport process modelling (Knyazikhin et al., 1998b; Verhoef and Bach, 2007). However, modelling soil reflectance is challenging due to the complex optical properties of soil in shortwave

bands. The GSV soil reflectance model addresses this by providing an effective method for approximating the reflectance spectra of both dry and wet soils (Jiang and Fang, 2019). Coupling GSV with SRT is critical because: (1) soil drives reflectance at low LAI (< 2), requiring precise spectral representation; (2) SRT resolves canopy heterogeneity unaddressed by homogeneous models; (3) slope effects jointly modulate soil exposure and canopy gap probability. GSV-SRTS integrates these via local slope coordinates and coupled soil-canopy radiation.

The GSV refers to the soil spectral vector, which can be obtained by integrating dry and wet soil data. The global soil reflectance matrix $R_{m \times l}$ can be expressed as follows (Jiang and Fang, 2019):

$$R_{m \times l} \approx U_{m \times m} \sum_{m \times l} V_{l \times l} \quad (18)$$

where m represents the number of dry soil samples; l represents the number of bands; and $R_{m \times l}$ represents the dry soil spectral matrix. $U_{m \times m}$, $\Sigma_{m \times l}$, and $V_{l \times l}$ can be calculated by the Python callable function *svd* (singular value decomposition).

Principal component analysis is used to obtain $\Sigma_{m \times n}$ and $V_{n \times l}$, where $V_{n \times l}$ takes the first few vectors. $U_{m \times m} \Sigma_{m \times n}$ can be written as $C_{1 \times (n+1)}$. For our GSV model, instead of m row vectors, $C_{1 \times (n+1)}$ is needed, which can be expressed as follows (Jiang and Fang, 2019):

$$C_{1 \times (n+1)} = R_{1 \times d} V_{(n+1) \times d}^{-1} \quad (19)$$

where $R_{1 \times d}$ represents the soil spectral data from the region of interest. The first several rows of $V_{(n+1) \times d}$ can account for the first n rows of $V_{(n+1) \times d}$ because we take the first several vectors through principal component analysis. The $n + 1$ row of $V_{(n+1) \times d}$ represents the vector of the n rows of wet soil and one soil spectral data of the study area. Finally, the reflectance spectrum of the soil background can be calculated as follows (Jiang and Fang, 2019):

$$R_{1 \times l} = C_{1 \times (n+1)} V_{(n+1) \times l} \quad (20)$$

where $R_{1 \times l}$ is the final soil spectral vector.

2.4 BRF Calculation

The discrete ordinates method, a standard approach for solving radiative transfer problems, was used to numerically solve the coupled SRTS system with its boundary conditions. The incoming radiation is parameterized by the total flux $F_{\text{dir+dif}}(\Omega_0)$ (Shabanov et al., 2000). The horizontal average intensities $\bar{I}(z, \Omega)$ and $U(z, \Omega)$ are divided into direct and diffuse components for computational solution. The final simulated BRF is calculated from the resulting upwelling radiation intensity at the canopy top ($z = 0$) for the viewing direction Ω_v :

$$\text{BRF}(\Omega_v, \Omega_s) = \frac{\pi \cdot \bar{I}(0, \Omega_v)}{F_{\text{dir}}(\Omega_s) + E_{\text{diff}}} \quad (21)$$

where $E_{\text{diff}} = \int_{2\pi} d_0(\Omega) |\cos \theta_v| d\Omega$ is the total diffuse irradiance on the horizontal plane.

3 Dataset

3.1 Strategy for Evaluating the Performance of the SRTS Model

To comprehensively evaluate the proposed GSV-SRTS model, the simulations were conducted as follows: First, the overall accuracy of GSV-SRTS was evaluated against DART using scatterplots to validate the model feasibility. Next, GSV-SRTS was compared with the typical mountain CR models to validate its advantage in various terrain and canopy conditions after incorporating the SRT theory and soil spectral vector. The angular distribution of GSV-SRTS was analyzed to reveal the response mechanism of terrain and canopy conditions to multi-angle observations. Finally, multi-resolution satellite imagery was used to evaluate model suitability in real mountainous areas.

3.2 Comparison of DART-based Simulation Models

The DART model is a highly regarded analysis tool utilized for modeling the transmission of radiation signals within soil-leaf-canopy systems (Gastellu-Etchegorry et al., 2012). It has the capability to accurately simulate the canopy reflectance in various types of terrain and canopy structures. During the validation of the model, DART simulations were used as the standard to assess the reliability of the GSV-SRTS model as well as other comparable models. In the virtual scenarios created by DART, specific parameters such as the solar zenith angle of 30° and solar azimuth angle of 0° were set. Additionally, to evaluate the performance of the model in multi-angle observations, the view zenith angle was varied from 0 to 60° , while the view azimuth angle ranged from 0 to 360° , encompassing the entire observation hemisphere. To investigate the accuracy of the model across different sloping surfaces, the slope angle was adjusted from 0 to 50° in increments of 10° , covering gentle, moderate, and steep slopes. The aspect was fixed at 0 , 90 , 180 and 270° , corresponding to surfaces facing north, east south and west respectively. Various values of Leaf Area Index (LAI) ranging from 0.5 to 4 , canopy height from 2 to 30 m, and canopy density from 0.1 to 0.8 were set to represent sparse, moderate, and dense vegetation coverage scenarios. The virtual vegetation scenes were standardized at $100\text{ m} \times 100\text{ m}$ with diverse canopy structures, terrains, and viewing conditions. The specifics of the input parameters for generating scenes in DART are outlined in Table 1. In comparison to traditional mountain canopy reflectance models, the SLCT and GOST2 models were utilized, which are based on radiative transfer and geometrical optical theories for sloping terrains. All results from the compared models were juxtaposed with the

DART simulations in the same virtual scenes as the benchmark for accuracy assessment.

3.3 Assessment of Canopy Structural Effects on Multi-angle Reflectance

To discover the influence of canopy structure, multi-angle CR simulations were conducted. The virtual vegetation scenes were set with stable terrain and view conditions. The sun zenith angle was set to 30° and the sun azimuth angle was set to 0° . The view zenith angle was set to range from 0 to 60° , and the view azimuth angle ranged from 0 to 360° to cover the hemispheric viewing space. And the canopy densities were set to 0.2 , 0.5 and 0.8 to demonstrate sparse, medium and dense vegetation coverage. On multi-angle CR simulations, the terrain and canopy condition effects were assessed explicitly.

3.4 Assessment of the Terrain and Canopy Conditions Effects on Multi-angle CR Simulations

To assess the effectiveness of the proposed model, it is imperative to simulate canopy reflectance in a real mountainous setting. The chosen location for this study is the Wanglang Field Observation Station, situated in the northeastern region of the Tibetan Plateau at coordinates approximately 32.94° N and 104.07° E . This area boasts a diverse landscape characterized by towering mountain peaks and deep gorges, with elevations ranging from 2000 to 4200 m and slopes that can vary from gentle inclines to steep gradients of up to 76° . The various vegetation types that thrive in this unique environment include deciduous forests, coniferous forests, mixed forests combining both coniferous and deciduous species, as well as scrublands. Field measurements were stratified by elevation, slope, and aspect to cover dominant vegetation types. Canopy parameters (LAI, height) were measured via hemispherical photography and UAV LiDAR, with soil spectra sampled from exposed sites aligned with target pixels.

Satellite products from Landsat 9-OLI, Sentinel-2, and Jilin-1 with spatial resolutions of 30 , 10 , and 0.5 m, respectively, are presented in Fig. 2. Cloud-free remote sensing images from these sensors, covering the experimental area, served as reference data for model performance assessment. The Landsat 9-OLI image was acquired on 30 July 2024, during the vegetation growing season, with solar zenith and azimuth angles of 25.5 and 119.6° , respectively. It was obtained from the Earth Resources Observation and Science (EROS) Center Science Processing Architecture (ESPA) on-demand interface (<https://espa.cr.usgs.gov/>, last access: 27 April 2026), which provides surface reflectance products corrected using the Second Simulation of the Satellite Signal in the Solar Spectrum Vector (6SV) model (Vermote et al., 2016). The Sentinel-2 image was captured on 8 July 2022, with corresponding solar zenith and azimuth angles of 18.73 and 119.2° , and was downloaded from the Copernicus

Table 1. Specification of the input parameters of the scenes generated by DART.

	Model Parameters	Units	Range
Leaf parameters			
S_L	Leaf linear characteristic dimension	[m]	0.05–0.2
anopy structure parameters			
LAI	Leaf area index	[m ² m ⁻²]	0.5–4
ALA	Average leaf angle	[°]	30
p	Canopy density	unitless	0.1–0.8
H	Canopy height	[m]	2–30
$\chi(x, y, z)$	Indicator function	unitless	0 or 1
Illumination view geometry			
θ_s	Sun zenith angle	[°]	0
θ_v	View zenith angle	[°]	0–360
φ_s	Sun azimuth angle	[°]	30
φ_v	View azimuth angle	[°]	0–60
Atmospheric condition			
f_{dir}	Diffuse radiation fraction	unitless	0.2
T	Atmospheric transmittance	unitless	0.7
Topographic factors			
θ_g	Slope	[°]	0–60
φ_g	Aspect	[°]	0–360

Open Access Hub (<https://dataspace.copernicus.eu/>, last access: 21 April 2026). The Jilin-1 remote sensing images were acquired and mosaicked from the Jilin-1 Satellite Network (<https://www.jl1mall.com/>, last access: 27 April 2026), with data collected between June and August from 2022 to 2024. These three remote sensing images are accompanied by corresponding digital elevation models (DEMs) for topographic analysis. Topographic factors for the study area were derived from the following sources: the ASTER Global Digital Elevation Model (GDEM) version 2 (spatial resolution of 1 arc-second, approximately 30 m) was used for the Landsat 9-OLI image; the Copernicus DEM GLO-10 product (10 m resolution) was acquired from the Copernicus Open Access Hub to match the Sentinel-2 image; and high-resolution DEM data were obtained via unmanned aerial vehicle (UAV) laser scanning and resampled to a 0.5 m resolution to align with the Jilin-1 imagery.

The input parameters for driving the SRTS model are summarized in Table 2. These parameters have been carefully defined using a combination of field measurements, remote sensing products, and relevant literature. For example, the leaf linear characteristic dimension (S_L) has been designated as 0.05–0.2 m based on typical values for vegetation (Jacquemoud et al., 2009). Canopy structure parameters included in the model consist of a leaf area index (LAI) ranging from 2–4 m² m⁻², canopy height (C_H) varying from 5–30 m to encompass the range of measurements, and an average leaf an-

gle (ALA) of 30° which follows an ellipsoidal distribution assumption (Campbell, 1990). In order to accurately capture the topographic variability of the study area, parameters such as slopes (θ_g) ranging from 0–60° and aspects (φ_g) from 0–360° have been incorporated into the model. These parameters ensure that the full terrain characteristics are taken into consideration during the simulations. Furthermore, atmospheric parameters for the study area have been derived using the MODTRAN atmospheric radiative transfer model (Berk et al., 2004). This ensures that the atmospheric conditions are accurately represented in the model simulations. The illumination geometry has been fixed based on remote sensing observations, providing a consistent and reliable input for the model. By incorporating all of these parameters into the SRTS model, we are able to accurately simulate and analyze the surface reflectance properties of the study area.

The input parameters for the model are outlined in Table 2, with a summary provided for reference. A dataset based on these parameters was used to generate 10 000 combinations of input values. Each combination was then used to compare the remote sensing reflectance with the simulated reflectance stored in a lookup table (LUT) on a pixel-by-pixel basis. In order to mitigate the challenges posed by the ill-posed nature of the model inversions (Vermote et al., 1997) the final outcome was determined by averaging the results from the 100 best-matching simulations. The degree of agreement between the observed and simulated reflectance was evaluated

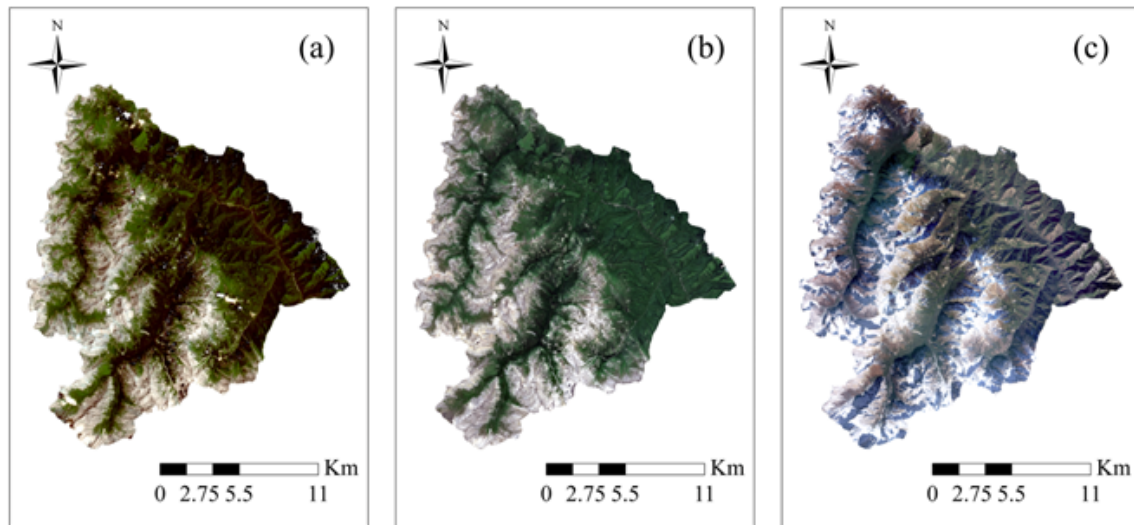


Figure 2. Study area Wanglang National Nature Reserve, Pingwu County, Mianyang with three different sources of remote sensing images, from which (a) Landsat9-OLI, (b) Sentinel2, (c) Jilin-1.

using the following cost function:

$$\text{Cost} = \sqrt{\left(\frac{\text{Sim}_r - \text{Obs}_r}{\text{Obs}_r}\right)^2 + \left(\frac{\text{Sim}_n - \text{Obs}_n}{\text{Obs}_n}\right)^2} \quad (22)$$

where Sim_r and Sim_n are the simulated reflectances in the red and NIR bands, respectively, and Obs_r and Obs_n are the observed reflectances in the red and NIR bands, respectively.

4 Results and analysis

4.1 Model Evaluation by DART and Typical CR Models

To validate the overall simulation accuracy of the GSV-SRTS model, the GSV-SRTS simulations were compared against the DART simulations. As shown in Figs. 3 and 4, the scatter plots were generated using comprehensive input parameter combinations, including varying slopes, aspects, canopy densities, and observation directions. The results showed that GSV-SRTS achieved the highest R^2 value of 0.9136 (0.9052) and the lowest RMSE of 0.0146 (0.0106) in the red (NIR) band, outperforming other compared models.

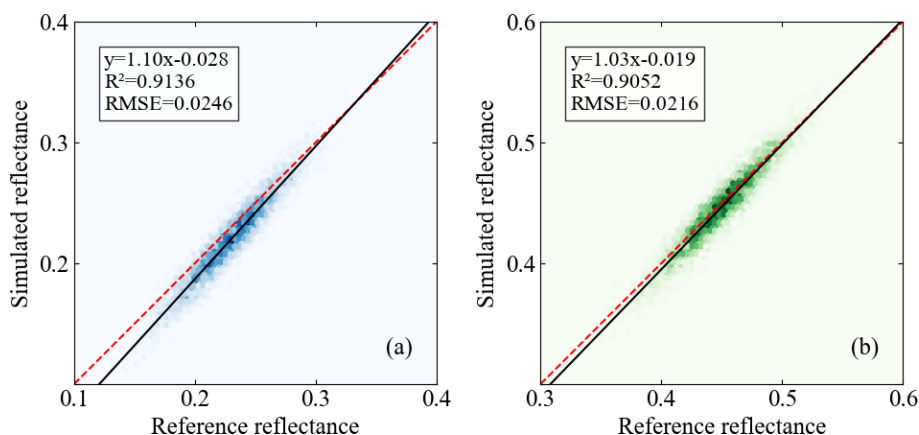
As shown in Fig. 4, the model comparison across different slopes shown that the GSV-SRTS and DART simulations have good consistency over different sloping terrains. In comparisons between DART and other models, the performance of GOST2 and SLCT deteriorates as slope increases. The SLCT model, which assumes trees grow perpendicular to the ground, exhibits distortions in simulating crown gap fraction on steeper slopes. This in turn affects the accurate characterization of radiation contributions over sloping terrain. GOST2 assumes that trees follow the Neyman type-A

distribution pattern (Fan et al., 2015). Although the GOST2 model can accurately describe the spatial distribution of the trees, the scenes generated by DART where trees are randomly distributed is more suitable for SRTS. Specifically, in the red (NIR) band, GSV-SRTS precision increases from 0.8702 (0.8635) at 0° to 0.9318 (0.9234) at slopes $\geq 30^\circ$. This comparison demonstrates enhanced capability of GSV-SRTS in complex terrain conditions.

To specifically compare the reflectance under different view zenith angles, the different slopes were set from 0 to 50° with an interval of 10° , as illustrated in Fig. 5. As the terrain slope increases, the GSV-SRTS model achieves the best match with DART simulations in the red and NIR bands, despite SLCT performing better on flat terrain. As the slope steepens, the fundamental differences in physical approach of each model become increasingly apparent. The SLCT model relies on the simplified plane-parallel RT theory, assuming homogeneous leaf distribution and ignoring slope-induced shadowing effects. This leads to systematic underestimation of multiple scattering contributions in steeper terrain. The GOST2 assumes that the trees follow the Neyman type-A distribution, so when view zenith angle is near nadir, the probability of observing the background is larger than that of the other compared models. The GSV-SRTS model accounts for terrain conditions by coupling a voxel-based canopy representation with a Monte Carlo photon-tracking approach, enabling it to resolve anisotropic scattering patterns caused by tilted surfaces. This ability to adjust and remain accurate even in more complex conditions makes GSV-SRTS especially well-suited for sloping terrains.

Table 2. Specification of the input parameters to generate the LUT.

	Model Parameters	Units	Range
Leaf parameters			
S_L	Leaf linear characteristic dimension	[m]	0.05–0.2
Canopy structure parameters			
LAI	Leaf area index	[m ² m ⁻²]	2–4
ALA	Average leaf angle	[°]	30
p	Canopy density	unitless	0.2–0.8
C_H	Canopy height	[m]	5–30
$\chi(x, y, z)$	Indicator function	unitless	0 or 1
Illumination view geometry			
θ_s	Sun zenith angle	[°]	25.5
θ_v	View zenith angle	[°]	0–360
φ_s	Sun azimuth angle	[°]	119.6
φ_v	View azimuth angle	[°]	0–60
Atmospheric condition			
f_{dir}	Diffuse radiation fraction	unitless	0.2
T	Atmospheric transmittance	unitless	0.7
Topographic factors			
θ_g	Slope	[°]	0–60
φ_g	Aspect	[°]	0–360

**Figure 3.** Density scatterplots between the canopy reflectance simulated by DART and the GSV-SRTS models. (a) and (b) represent the DART simulations compared with the SRTS model in the red and NIR bands.

4.2 Terrain Effects on CR in Hemispheric Space

To reveal the effects of terrain factors and viewing conditions to canopy reflectance, the angular distributions of reflectance under various scenarios were simulated by the GSV-SRTS model. The results are presented in the form of polar coordinate maps. In these maps, the radial distance corresponds to the zenith angle, while the angular position represents the viewing azimuth angle. The polar contour maps for the red and NIR bands are displayed in Figs. 6 and 7, respectively.

As shown in Fig. 6, reflectance in the red band ranges primarily between 0.07 and 0.19. The peak of reflectance occurs at the hotspot, where the view zenith angle is 30° and the azimuth angle is 0°. At the same azimuth angle, reflectance decreases as the zenith angle increases. This angular dependence occurs due to geometric shadowing, path length effects and volume scattering reduction. Photons penetrating the canopy at off-nadir angles traverse longer effective path lengths through the vegetation medium, enhancing absorption by the canopy.

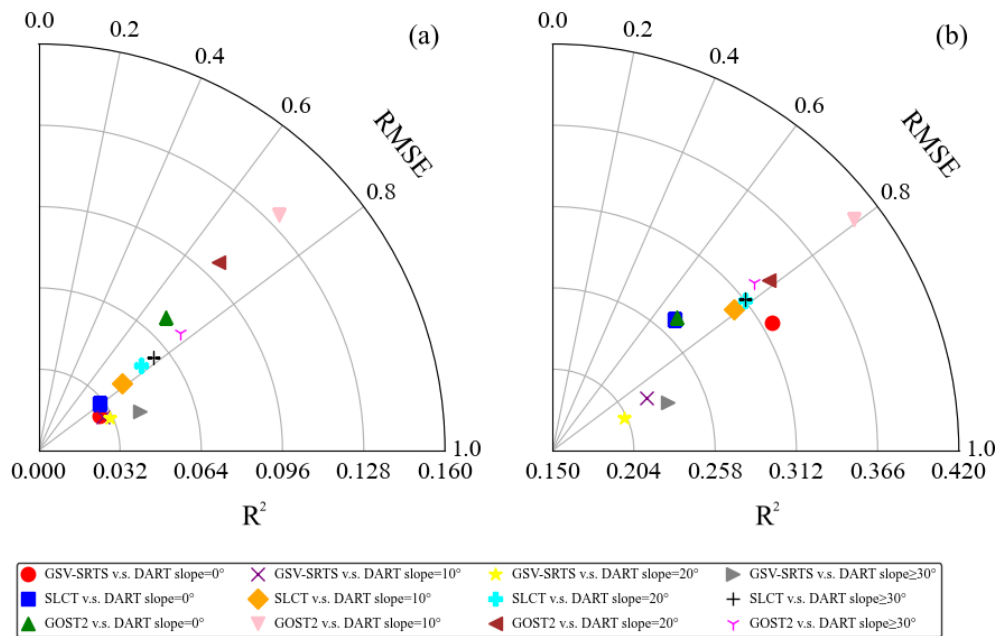


Figure 4. The comparison between GSV-SRTS, SLCT, GOST2, and DART over different sloping terrains. (a) and (b) represent the results in the red and NIR bands, respectively.

When the aspect is 0° (facing the illumination direction), increasing the slope expands the high-reflectance zone and intensifies maximum reflectance at the azimuth angle of 0°. This amplification occurs because steeper slopes facing the light source create optimal conditions for enhanced canopy reflectance. The tilted surface exposes a larger area to direct solar radiation, enhancing the sunlight received by slope-facing vegetation by a factor of $1/\cos\theta$ (where θ is slope angle) (Dubayah and Rich, 1995). On the slope of 20°, solar radiation increases by 64 % compared to that in flat terrain.

However, when the slope reaches 20° and the aspect shifts to 90° (panel g) or 270° (panel i), high reflectance concentrates in specific sections of the upper hemisphere. Reflectance is higher between azimuth angles of 0–90° in panel (g) and 270–360° in panel (i) because the probability of sunlight reaching the ground becomes larger. For slopes with an aspect of 90°, maximum reflectance occurs when the solar azimuth angle is approximately 90°. The PP (principal plane) of incidence is the same with the normal vector of the slope, minimizing the shadowing effects. This geometry enhances the backscatter direction observed by the sensor. It also creates minimal cast shadows and maximum visible illuminated areas, increasing the apparent reflectance. Similarly, slopes with a 270° aspect exhibit peak reflectance near a solar azimuth angle of 270°, following the same geometric principle. Notably, polar contour maps of a 20° slope with aspects of 90 and 270° exhibit symmetry about the vertical axis. This symmetry stems from the fact that the relative azimuth angle between the illumination and viewing directions is the same in both instances. When the sun-sensor geometry

is fixed, the reflectance remains consistent, showing mirror-like symmetry around the azimuth of 0°. This confirms that light interacts with slopes in the same way, regardless of their facing direction.

In the NIR band, reflectance displays similar trends yet maintains consistently higher values relative to the red band. As shown in Fig. 7, reflectance ranges primarily from 0.31 to 0.56, with higher values compared to the red band. This difference primarily stems from reduced chlorophyll absorption in the NIR spectrum, enabling more effective light penetration through multiple canopy layers. These distinct interactions lead to characteristically higher NIR reflectance and lower red reflectance in vegetation canopies.

When the slope is 20° with the aspect of 90 or 270°, canopy reflectance increases in the hemispherical distribution at the small zenith angles. This demonstrates that steeper slopes facing the sunward direction receive more solar illumination. The consistent slope and illumination direction, combined with symmetrical aspect, result in a symmetrical distribution of gap fractions, which in turn leads to a symmetrical hemispherical reflectance distribution. For a terrain characterized by the slope of 20° facing the aspect of 90°, lower reflectance is concentrated along the 90–180° view azimuth angles. In contrast, when the aspect shifts to 270°, reflectance decreases along the 180–270° view azimuth directions. When the slope faces 90°, sensors viewing along the azimuths of 90–180° observe the sunlit slope but detect reduced reflectance. Because when the solar azimuth equals aspect, the illumination angle on the inclined surface is minimized, reducing casting shadows and increasing the pro-

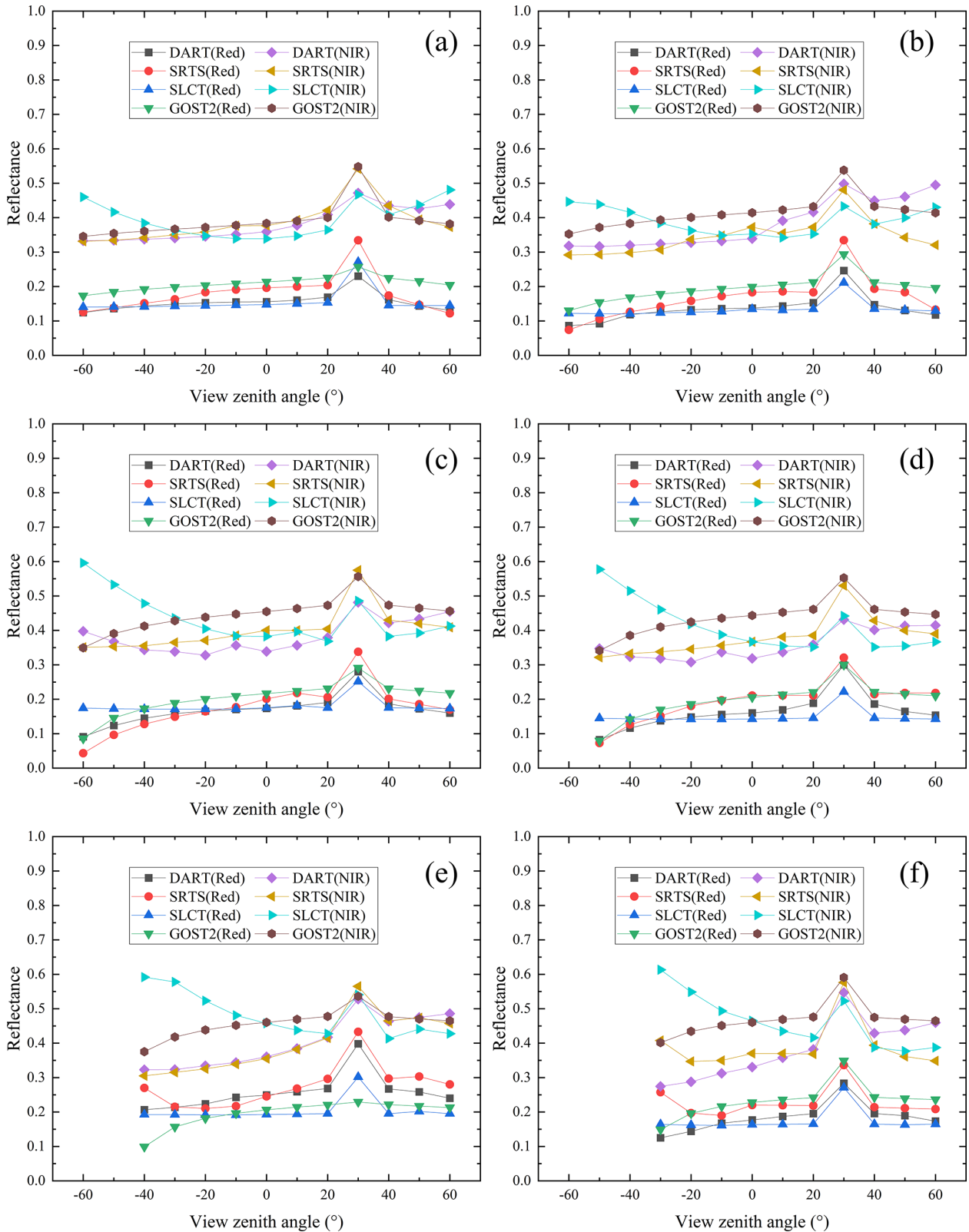


Figure 5. Comparison of canopy reflectance simulated by SRTS, SLCT, and GOST2 models in the PP (principal plane) for slopes of (a) 0°, (b) 10°, (c) 20°, (d) 30°, (e) 40°, and (f) 50°. A view azimuth angle of 0° corresponds to the positive X axis direction, while 180° corresponds to the negative X axis direction.

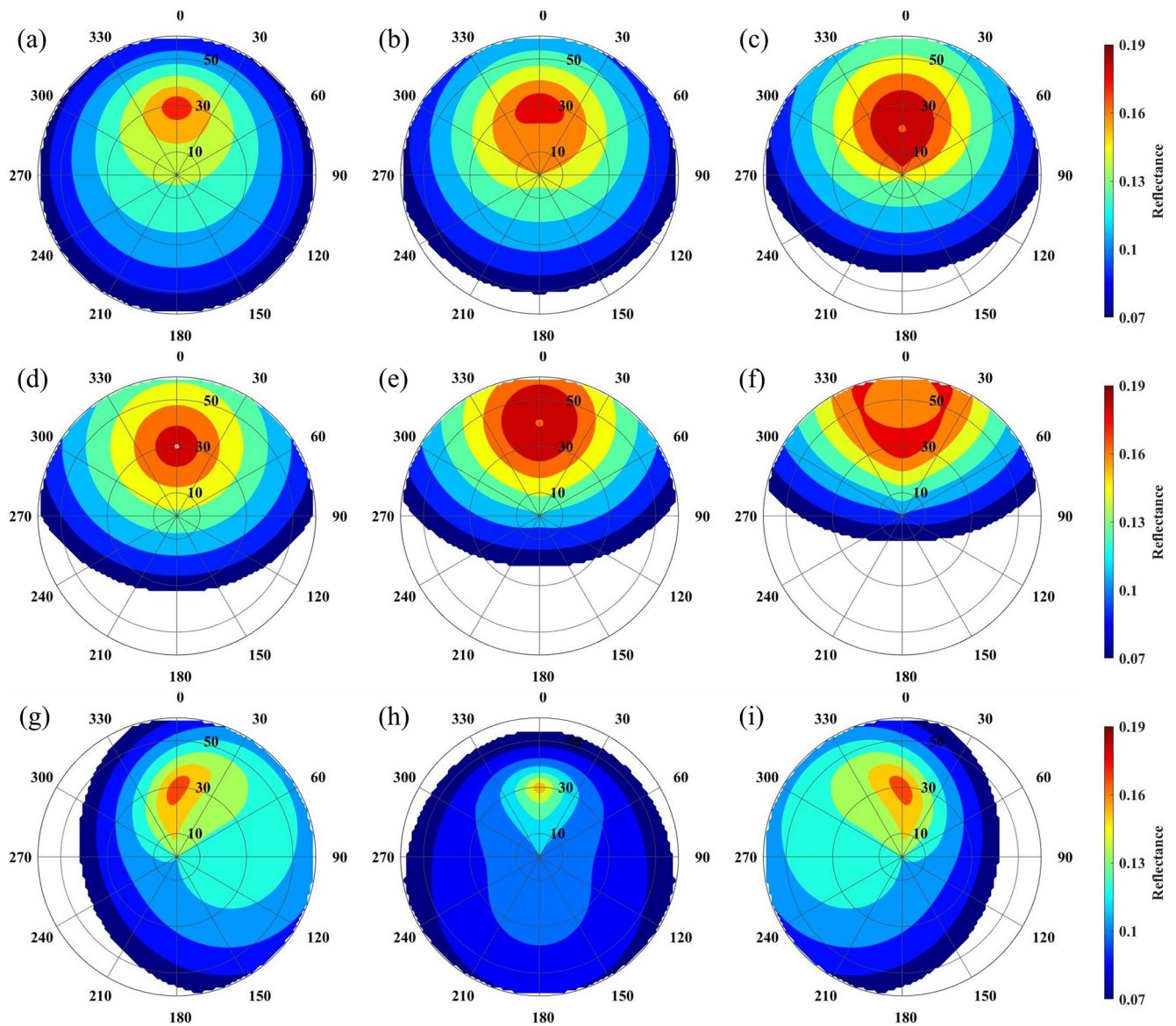


Figure 6. Angular distribution of canopy reflectance in the red band: (a–f) for an aspect of 0° and slopes of 0, 10, 20, 30, 40, and 50° ; (g–i) for a slope of 20° and aspects of 90° , 180° , and 270° .

jected sunlit area. This geometry enhances the backscattering direction observed by sensors. The same physical principles apply to the aspect of 270° , where reflectance maxima occur near solar azimuth of 270° , demonstrating symmetrical behaviour across the PP.

While the hotspot fundamentally results from aligned sun-view geometry reducing mutual shadowing, sloping terrain distorts its signature: local solar/view angles (Eq. 1) shift peak reflectance toward the illuminated slope face, amplified by topographic modulation (Eq. 5). GSV-SRTS resolves this by coupling slope-corrected geometry with stochastic gap probability, capturing asymmetric hotspot broadening on inclined surfaces.

These results demonstrated the importance of incorporating topographic factors into GSV-SRTS in mountainous conditions, where terrain-induced factors, solar and view geometries significantly affect canopy reflectance patterns. The ability of GSV-SRTS to account for terrain-related variations ensures more accurate RT process simulations.

4.3 Gap Probabilities Effects on Surface Reflectance in Hemispheric Space

The gap probability, a critical factor influencing the radiative properties of vegetation and soil in remote sensing applications, was utilized in a study to investigate how canopy structure impacts surface reflectance simulations. Using the

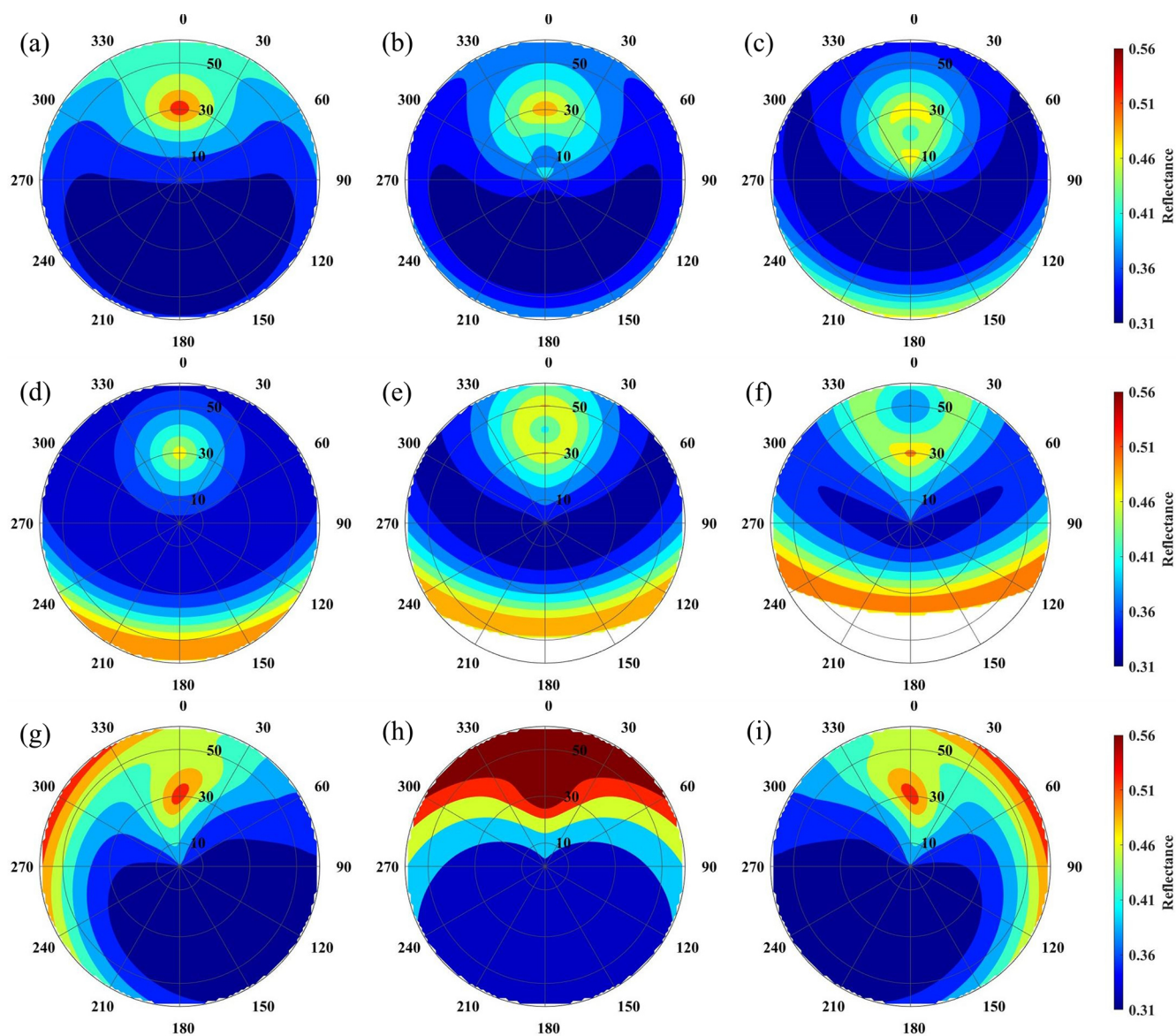


Figure 7. Angular distribution of canopy reflectance in the NIR band: (a–f) for an aspect of 0° and slopes of 0, 10, 20, 30, 40, and 50° ; (g–i) for a slope of 20° and aspects of 90° , 180° , and 270° .

GSV-SRTS model, the hemispherical distributions of surface reflectance in the red and NIR bands were simulated under different canopy densities. Figure 8 illustrates that canopy reflectance peaks in the hotspot direction, regardless of changes in slope. This directional peak is a result of decreased canopy densities and shadowing from the ground when the sensor's viewing angle aligns with the direction of solar illumination. The GSV-SRTS model accurately captures the reduced probability of observing shaded areas by integrating terrain-modified gap probability and geometries into its simulations. Increasing canopy density leads to a noticeable increase in NIR reflectance (panels b, d, and f) particularly at the nadir, due to enhanced photon interactions

within the canopy and changes in gap probability affecting radiation penetration. In contrast, red band reflectance (panels a, c, and e) remains low across all canopy densities, reflecting the strong absorption of red light by chlorophyll. Therefore, both spectral regions demonstrate significant bidirectional reflectance distribution function (BRDF) effects, with NIR reflectance being more sensitive to changes in canopy density.

Moreover, reflectance in the backward-scattering direction consistently exceeds that in the forward-scattering direction. This indicates sunlit crowns become more visible at this direction and mutual shading effects are minimized in this viewing geometry, where the sunlit portions dominate

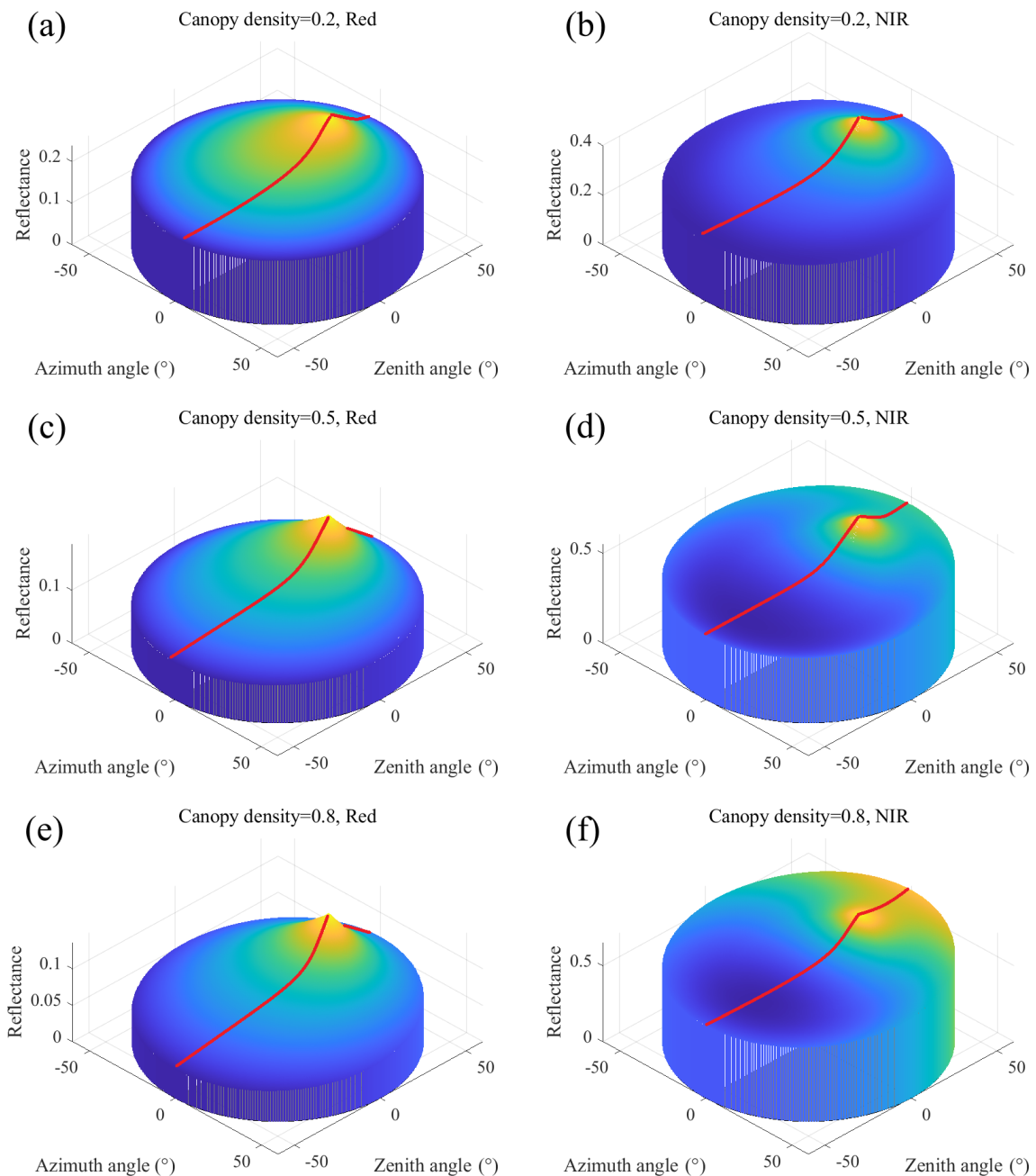


Figure 8. Hemispheric views of GSV-SRTS-simulated reflectance over three different canopy densities (**a, b**) 0.2, (**c, d**) 0.5 and (**e, f**) 0.8. The left column represents the canopy reflectance in the red band, and the right column represents the canopy reflectance in the NIR band.

the field of view of sensors. Such directional reflectance features are especially pronounced under dense canopies, where shadowing and multiple scattering further enhance the contrast between forward and backward observations. These reflectance characteristics provide critical understanding of the 3D structure and complexity of forest canopies.

4.4 Model Assessment in a Real Mountainous Region

To assess the effectiveness of the GSV-SRTS model in a practical mountainous setting and explore how well the model works at different levels of detail, we utilized a combination of satellite imagery sources with varying resolutions. Specifically, the Landsat 9-OLI imagery with a resolution of 30 m, the Sentinel-2 imagery with a resolution of 10 m, and the Jilin-1 imagery with a resolution of 0.5 m were employed

to establish the reference reflectance values for our model evaluation. Additional information regarding the specific geographic area of focus for our study and the technical details of the images can be found in Sect. 3.4.

As illustrated in Fig. 9, the GSV-SRTS-simulated reflectance shows lower R^2 values of 0.7129 (0.7287) and higher RMSE values of 0.0291 (0.0376) in the red (NIR) band when compared with the Landsat9-OLI image reflectance. For the Sentinel-2 image, the SRTS-simulated reflectance achieves R^2 values of 0.8067 (0.8097) and RMSE values of 0.0271 (0.0292) in the red (NIR) band. The SRTS-simulated reflectance shows the highest consistency with the reflectance of the JiLin-1 image, with R^2 values of 0.9078 (0.9143) and RMSE values of 0.0201 (0.0212) in the red (NIR) band.

Even for medium-low resolution pixels, GSV-SRTS maintains advantages by statistically aggregating sub-pixel heterogeneity into radiative parameters, avoiding homogenization biases. Its terrain-aware structure ensures accurate BRDF shapes on slopes, where homogeneous models exhibit systematic errors. However, the reflectance simulation accuracy of the GSV-SRTS model enhances with higher spatial resolution of remote sensing images, owing to the ability of the underlying SRT theory and GSV model to resolve finer details in microscale settings. This compatibility stems from the core mechanics of the GSV-SRTS model, which simulates photon interactions within the canopy in detail. The model incorporates key processes, including multiple scattering between leaves, leaf orientation, shadowing effects, and canopy structure variation. And the soil background is fully considered and accurately modelled. Consequently, the GSV-SRTS model is highly compatible with high-resolution imagery. In contrast, coarser resolution images tend to smooth out small-scale features, limiting the ability of the model to leverage its detailed photon-tracking capabilities. This limitation is clearly evidenced by the lower R^2 values obtained with Sentinel-2 and Landsat 9-OLI data, which are primarily attributed to the homogenization of intra-pixel spatial details – terrain variation, canopy structure, and soil background – during the pixel integration process. Our model simulates these sub-pixel heterogeneities explicitly, but the validation data from medium-resolution sensors represents an aggregated average. This does not diminish the model's utility for coarser resolutions; rather, it highlights that the GSV-SRTS model is particularly advantageous for applications where understanding or quantifying the impact of sub-pixel heterogeneity is essential, such as in scaling studies, high-fidelity scene simulation, or informing the parameterization of larger-scale biogeophysical models. As a result, the GSV-SRTS model achieves optimal accuracy with high-resolution images, producing more realistic reflectance estimates. Therefore, the integration of high-resolution data with the photon-sensitive framework of the GSV-SRTS model enables precise capture of subtle canopy reflectance variations,

optimizing model performance and achieving highly precise results.

As a result, the GSV-SRTS model achieves optimal accuracy with high-resolution images, producing more realistic reflectance estimates. Therefore, the integration of high-resolution data with the photon-sensitive framework of the GSV-SRTS model enables precise capture of subtle canopy reflectance variations, optimizing model performance and achieving highly precise results.

5 Discussion

Accurate modeling of soil-canopy radiation interactions is essential for retrieving biophysical variables at regional-to-global scales. However, topographic relief and heterogeneous landscapes introduce significant uncertainties in radiative transfer simulations. While numerous canopy reflectance models account for sloping terrain, most cannot take heterogeneities of canopy structure and soil properties into account, leading to distorted BRDF patterns (Li et al., 1993; Gastellu-Etcheberry et al., 1996; Chen and Leblanc, 1997). This study proposed a CR model by extending the GSV and the stochastic RT model for Sloping Terrains (GSV-SRTS), improving the model applicability in real mountainous environments. The GSV-SRTS model advances vegetation and soil reflectance modeling because of its physically based BRDF framework, which intrinsically accounts for 3D canopy structure and surface interactions (Widlowski et al., 2015).

However, the study still has limitations in the theoretical framework and experimental design, requiring further improvement. Although the GSV-SRTS model incorporates terrain effects, the influence of the surrounding terrains was not fully considered. In mountainous regions, varying slope angles significantly affect RT by altering shadow patterns, neglecting the adjacent terrain irradiance may increase inaccuracies in remote sensing modeling, especially for the surface coverage with high reflectance (Mousivand et al., 2015; Rich and M., 1995; Sandmeier and Itten, 1997). The surrounding terrains may block direct solar radiation, reducing incident energy on the target surface (Riaño et al., 2003). Surrounding terrain surfaces scatter indirect radiation, altering the total flux received by the canopy (Gu and Gillespie, 1998). Concave landforms (e.g., valleys) enhance multiple reflections, while convex features (e.g., ridges) redistribute local energy budgets (Soenen et al., 2005; Chen and Black, 1992). Future studies should explore integrating surrounding terrain effects into the GSV-SRTS model to enhance accuracy under different terrains (Knyazikhin et al., 1998a).

The General Spectral Vector (GSV) was originally derived from the LUCAS global soil database, which comprises reflectance spectra from 19 036 dry soil samples (Jiang and Fang, 2019). While this dataset provides a robust foundation for modeling soil optical properties, its applicability

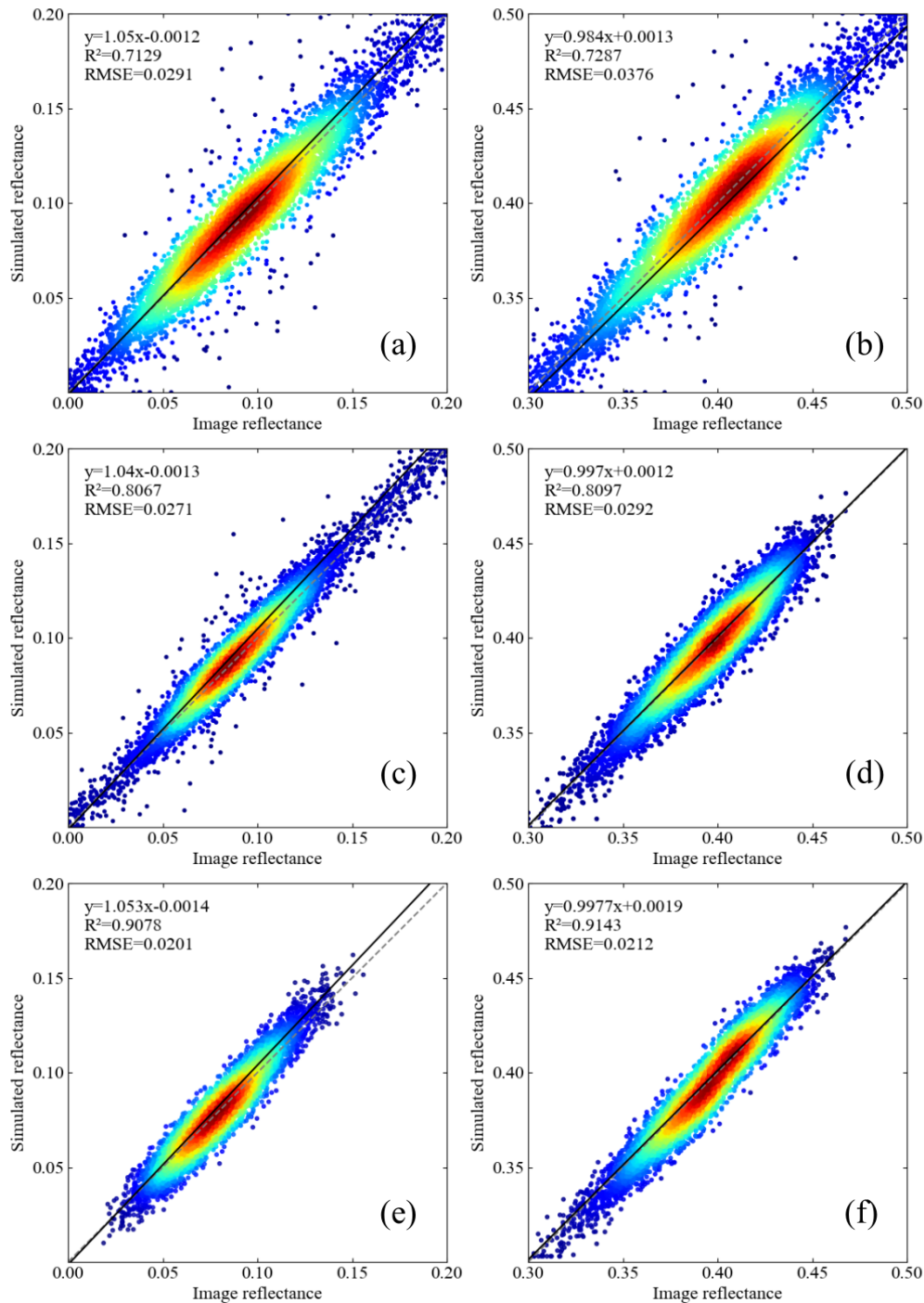


Figure 9. Density scatterplots comparing the simulated reflectance from the SRTS model with the image reflectance for (a) red and (b) NIR bands of Landsat 9-OLI, (c) red and (d) NIR bands of Sentinel-2, and (e) red and (f) NIR bands of Jilin-1.

to larger-scale or diverse regional studies remains limited due to geographical and pedological constraints. To enhance the generalizability and accuracy of the GSV-PROSAILT model across varied ecosystems and soil types, it is essential to expand the GSV framework by incorporating a broader and more diverse set of soil samples. This expansion would

strengthen the model's utility for vegetation-soil radiative transfer modeling by enabling a more accurate representation of spatial variability in soil composition, moisture content, and surface conditions. As emphasized by Jiang and Fang (2019), extending the spectral library with additional representative samples is a critical step toward achieving higher

predictive performance and broader operational applicability in remote sensing applications.

The topographic influence on canopy reflectance is channeled through two primary, interconnected physical mechanisms in the model: (i) the modification of the effective extinction coefficient due to changes in the relative pathlength through the canopy per unit vertical depth in the local slope coordinates, and (ii) the alteration of the canopy gap probability, modeled via the PCF within the stochastic framework, which is sensitive to the terrain-modified illumination direction. The first governs the bulk attenuation of direct radiation along its path, while the second determines the probability of direct beam penetration to the soil or lower canopy layers. These two effects are not independent; the altered pathlength directly influences the spatial statistics that underpin the gap probability calculation. Our integrated approach through the local slope coordinate system ensures both effects are consistently accounted for, providing a more complete representation of terrain role in mountain canopy radiative transfer.

The current model uses a simplified pair-correlation function (PCF) to represent vegetation spatial structures, reducing computational demands. However, higher-order moments (e.g., three- or four-point correlation functions) in canopy structure could improve radiative characteristic predictions (Huang et al., 2008; Tang et al., 2014; Lewis and Disney, 2007). To accurately handle the radiative transfer under such complex scattering conditions, the model applies the discrete ordinates method with N_μ (polar) and N_φ (azimuthal) angles to discretize scattering integrals. The resulting coupled SRTE system is solved iteratively with Gauss-Seidel updates until intensity residuals fall below 10^{-4} , ensuring stability and energy conservation when using slope-modified coefficients. Although integrating higher-order moments would increase computational load, advancements in parallel computing and GPU technology provide potential solutions (Jonckheere et al., 2004; Lovell et al., 2003).

Moreover, field sampling efforts are hampered by the complex terrain and hindered by the dense vegetation cover within the study area. Increasing observation frequency and optimizing sampling schemes could enhance data representativeness (Lefsky et al., 2002). However, obtaining the canopy structure parameters in mountainous areas is challenging, which can refine the RT mechanisms (Zhao et al., 2009). Integrating advanced sensing techniques like LiDAR provide a feasible solution for addressing these limitations (Yang et al., 2018; Bailey et al., 2020).

6 Conclusion

This study proposes a canopy reflectance model, the GSV-SRTS model, which is based on the extended GSV and stochastic radiative transfer theory. The model is designed to accurately analyse canopy reflectance in sloping heterogeneous landscapes. To assess the effectiveness of the GSV-

SRTS model, comparisons were made with DART simulations, typical CR models, and remote sensing observations with multiple spatial resolutions. The results of the study indicate that the GSV-SRTS model adequately captures the variations in canopy reflectance induced by terrain and vegetation conditions. It exhibits strong consistency with DART benchmarks, with the DART benchmarks ($R^2 = 0.9136$ (0.9052), RMSE = 0.0246 (0.0216) in the red (NIR) band). And this study revealed the influences of various terrain and vegetation conditions on multi-angle CR simulations. By comparing the GSV-SRTS model with remote sensing observations, it was found that the model is suitable for soil-canopy radiative transfer modelling in small-scale scenes, with RMSE (R^2) values of 0.0201 (0.9078) for the red band and 0.0212 (0.9143) for the NIR band. Therefore, the development of the GSV-SRTS model provides a feasible paradigm for CR modeling and can be used as a potential tool biophysical parameter retrieval.

Code and data availability. The current version of GSV-SRTS code and dataset is available from figshare website <https://doi.org/10.6084/m9.figshare.30392938> (Li, 2025).

Author contributions. Conceptualization, GH and SL; methodology, JB and GH; software, SL and CL; validation, RY and JT; formal analysis, SL; investigation, SL and CL; resources, GH and SL; data curation, JT and RY; writing – original draft preparation, SL; writing – review and editing, GH; visualization, SL; supervision, JB; project administration, SL; funding acquisition, GH, RY, SL and JB.

Competing interests. The contact author has declared that none of the authors has any competing interests.

Disclaimer. Publisher's note: Copernicus Publications remains neutral with regard to jurisdictional claims made in the text, published maps, institutional affiliations, or any other geographical representation in this paper. The authors bear the ultimate responsibility for providing appropriate place names. Views expressed in the text are those of the authors and do not necessarily reflect the views of the publisher.

Acknowledgements. The authors give their appreciation to Dr. J.-P. Gastellu-Etchegorry for the valuable support of discrete anisotropic radiative transfer (DART) software; the Landsat 9 OLI image published by the Earth Resources Observation and Science Center Science Processing Architecture (ESPA); the Global Digital Elevation Model (DEM) Version 3 product by the Advanced Spaceborne Thermal Emission and Reflection Radiometer (ASTER); Jilin-1 remote sensing data by the China Changguang Satellite Technology Co., Ltd.

Financial support. This research was funded by the National Natural Science Foundation project of China (grant no. 42401425), the General Program of National Natural Science Foundation of China (grant no. 42465006), the National Key Research and Development Program of China (grant no. 2020YFA0608702), and the Science and Technology Research Program of Institute of Mountain Hazards and Environment, Chinese Academy of Sciences (grant no. IMHE-CXTD-03).

Review statement. This paper was edited by Cenlin He and reviewed by two anonymous referees.

References

- Bailey, B. N., Ponce de León, M. A., and Krayenhoff, E. S.: One-dimensional models of radiation transfer in heterogeneous canopies: a review, re-evaluation, and improved model, *Geosci. Model Dev.*, 13, 4789–4808, <https://doi.org/10.5194/gmd-13-4789-2020>, 2020.
- Baret, F., Jacquemoud, S., and Hanocq, J.-F.: The soil line concept in remote sensing, *Remote Sensing Reviews*, 7, 65–82, 1993.
- Berk, A., Anderson, G. P., Acharya, P. K., Bernstein, L. S., and Lewis, P. E.: MODTRAN5: a reformulated atmospheric band model with auxiliary species and practical multiple scattering options, *Proc. SPIE*, 5425, 341–347, 2004.
- Bird, R. E. and Hulstrom, R. L.: A simplified clear sky model for direct and diffuse insolation on horizontal surfaces, *Solar Energy Research Inst., Golden, CO, USA, SERI/TR-642-761*, <https://doi.org/10.2172/6510849>, 1981.
- Campbell, G. S.: Derivation of an angle density function for canopies with ellipsoidal leaf angle distributions, *Agr. Forest Meteorol.*, 49, 173–176, 1990.
- Chen, J. M. and Black, T. A.: Defining leaf area index for non-flat leaves, *Agr. Forest Meteorol.*, 15, 421–429, 1992.
- Chen, J. M. and Leblanc, S. G.: A four-scale bidirectional reflectance model based on canopy architecture, *IEEE T. Geosci. Remote*, 35, 1316–1337, 1997.
- Combal, B., Isaka, H., and Trotter, C.: Extending a turbid medium BRDF model to allow sloping terrain with a vertical plant stand, *IEEE T. Geosci. Remote*, 38, 798–810, <https://doi.org/10.1109/36.842009>, 2000.
- Dirac, P. A. M.: *The principles of quantum mechanics*, 27, Oxford University Press, ISBN 978-0-19-852011-5, 1981.
- Dubayah, R. and Rich, P. M.: Topographic solar radiation models for GIS, *Int. J. Geogr. Inf. Syst.*, 9, 405–419, 1995.
- Fan, W., Chen, J. M., Weimin, J., and Gaolong, Z.: GOST: A Geometric-Optical Model for Sloping Terrains, *IEEE T. Geosci. Remote*, 52, 5469–5482, <https://doi.org/10.1109/tgrs.2013.2289852>, 2014.
- Fan, W., Li, J., and Liu, Q.: GOST2: The Improvement of the Canopy Reflectance Model GOST in Separating the Sunlit and Shaded Leaves, *IEEE J. Sel. Top. Appl.*, 8, 1423–1431, <https://doi.org/10.1109/jstars.2015.2413994>, 2015.
- Gastellu-Etchegorry, J.-P., Demarez, V., Pinel, V., and Zagolski, F.: Modeling radiative transfer in heterogeneous 3-D vegetation canopies, *Remote Sens. Environ.*, 58, 131–156, 1996.
- Gastellu-Etchegorry, J.-P., Grau, E., and Lauret, N.: DART: A 3D model for remote sensing images and radiative budget of earth surfaces, in: *Modeling and Simulation in Engineering*, edited by: Alexandru, C., InTech, Rijeka, Croatia, <https://doi.org/10.5772/31315>, 2012.
- Gu, D. and Gillespie, A.: Topographic Normalization of Landsat TM Images of Forest Based on Subpixel Sun–Canopy–Sensor Geometry, *Remote Sens. Environ.*, 64, 166–175, 1998.
- Hu, G. and Li, A.: BOST: A Canopy Reflectance Model Suitable for Both Continuous and Discontinuous Canopies Over Sloping Terrains, *IEEE T. Geosci. Remote*, 60, 1–19, <https://doi.org/10.1109/tgrs.2022.3226460>, 2022.
- Huang, D., Knyazikhin, Y., Wang, W., Deering, D. W., Stenberg, P., Shabanov, N., Tan, B., and Myneni, R. B.: Stochastic transport theory for investigating the three-dimensional canopy structure from space measurements, *Remote Sens. Environ.*, 112, 35–50, 2008.
- Jacquemoud, S., Verhoef, W., Baret, F., Bacour, C., Zarco-Tejada, P. J., Asner, G. P., François, C., and Ustin, S. L.: PROSPECT+SAIL models: A review of use for vegetation characterization, *Remote Sens. Environ.*, 113, S56–S66, 2009.
- Jiang, C. and Fang, H.: GSV: a general model for hyperspectral soil reflectance simulation, *Int. J. Appl. Earth Obs.*, 83, <https://doi.org/10.1016/j.jag.2019.101932>, 2019.
- Jonckheere, I., Fleck, S., Nackaerts, K., Muys, B., Coppin, P., Weiss, M., and Baret, F.: Review of methods for in situ leaf area index determination: Part I. Theories, sensors and hemispherical photography, *Agr. Forest Meteorol.*, 121, 19–35, 2004.
- Knyazikhin, Y., Martonchik, J. V., Myneni, R. B., Diner, D. J., and Running, S. W.: Synergistic algorithm for estimating vegetation canopy leaf area index and fraction of absorbed photosynthetically active radiation from MODIS and MISR data, *J. Geophys. Res.-Atmos.*, 103, 32257–32275, 1998a.
- Knyazikhin, Y., Martonchik, J. V., Diner, D. J., Myneni, R. B., Verstraete, M., Pinty, B., and Gobron, N.: Estimation of vegetation canopy leaf area index and fraction of absorbed photosynthetically active radiation from atmosphere-corrected MISR data, *J. Geophys. Res.-Atmos.*, 103, 32239–32256, <https://doi.org/10.1029/98jd02461>, 1998b.
- Lefsky, M. A., Cohen, W. B., Parker, G. G., and Harding, J. D.: Lidar Remote Sensing for Ecosystem Studies, *Bioscience*, 52, 19–30, 2002.
- Lewis, P. and Disney, M.: Spectral invariants and scattering across multiple scales from within-leaf to canopy, *Remote Sens. Environ.*, 109, 196–206, 2007.
- Li, S.: GSV-SRTS model, figshare [code, data set], <https://doi.org/10.6084/m9.figshare.30392938>, 2025.
- Li, X., Strahler, A. H., and Woodcock, C. E.: A hybrid geometric optical-radiative transfer approach for modeling albedo and directional reflectance of discontinuous canopies, *IEEE T. Geosci. Remote*, 33, 466–480, <https://doi.org/10.1109/TGRS.1995.8746028>, 1995.
- Li, X., Huang, H., Shabanov, N. V., Chen, L., Yan, K., and Shi, J.: Extending the stochastic radiative transfer theory to simulate BRDF over forests with heterogeneous distribution of damaged foliage inside of tree crowns, *Remote Sens. Environ.*, 250, 112040, <https://doi.org/10.1016/j.rse.2020.112040>, 2020.
- Lovell, J. L., Jupp, D. L. B., and Culvenor, D. S.: Using airborne and ground-based ranging lidar to measure canopy struc-

- ture in Australian forests, *Can. J. Remote Sens.*, 29, 607–622, <https://doi.org/10.5589/M03-026>, 2003.
- Mousivand, A., Verhoef, W., Menenti, M., and Gorte, B.: Modeling top of atmosphere radiance over heterogeneous non-Lambertian rugged terrain, *Remote Sens.-Basel*, 7, 8019–8044, 2015.
- Nocita, M., Stevens, A., van Wesemael, B., Aitkenhead, M., Bachmann, M., Barthès, B., Dor, E. B., Brown, D. J., Clairotte, M., and Csorba, A.: Soil spectroscopy: an alternative to wet chemistry for soil monitoring, *Adv. Agron.*, 132, 139–159, 2015.
- Pinheiro, É. F., Ceddia, M. B., Clingensmith, C. M., Grunwald, S., and Vasques, G. M.: Prediction of soil physical and chemical properties by visible and near-infrared diffuse reflectance spectroscopy in the central Amazon, *Remote Sens.-Basel*, 9, 293, <https://doi.org/10.3390/rs9040293>, 2017.
- Riaño, D., Chuvieco, E., Salas, J., and Aguado, I.: Assessment of different topographic corrections in Landsat-TM data for mapping vegetation types (2003), *IEEE T. Geosci. Remote*, 41, 1056–1061, 2003.
- Ross, J.: The radiation regime and architecture of plant stands, Springer Science & Business Media, <https://doi.org/10.1007/978-94-009-8647-3>, 2012.
- Roujean, J. L., Leroy, M., and Deschamps, P. Y.: A bidirectional reflectance model of the Earth's surface for the correction of remote sensing data, *J. Geophys. Res.-Atmos.*, 97, 20455–20468, 1992.
- Sandmeier, S. and Itten, K. I.: A physically-based model to correct atmospheric and illumination effects in optical satellite data of rugged terrain, *IEEE T. Geosci. Remote*, 35, 708–717, 1997.
- Schaaf, C. B., Li, X., and Strahler, A. H.: Topographic effects on bidirectional and hemispherical reflectances calculated with a geometric-optical canopy model, *IEEE T. Geosci. Remote*, 32, 1186–1193, <https://doi.org/10.1109/36.338367>, 1994.
- Shabanov, N. V., Knyazikhin, Y., Baret, F., and Myneni, R. B.: Stochastic modeling of radiation regime in discontinuous vegetation canopies, *Remote Sens. Environ.*, 74, 125–144, 2000.
- Shabanov, N. V., Huang, D., Knjazikhin, Y., Dickinson, R., and Myneni, R. B.: Stochastic radiative transfer model for mixture of discontinuous vegetation canopies, *J. Quant. Spectrosc. Ra.*, 107, 236–262, 2007.
- Soenen, S. A., Peddle, D. R., and Coburn, C. A.: SCS+C: a modified Sun-canopy-sensor topographic correction in forested terrain, *IEEE T. Geosci. Remote*, 43, 2148–2159, <https://doi.org/10.1109/tgrs.2005.852480>, 2005.
- Tang, H., Dubayah, R., Brolly, M., Ganguly, S., and Zhang, G.: Large-scale retrieval of leaf area index and vertical foliage profile from the spaceborne waveform lidar (GLAS/ICESat), *Remote Sens. Environ.*, 154, 8–18, 2014.
- Vainikko, G.: Transfer approach to the mean intensity of radiation in non-continuous clouds, *Trudy MGK SSSR, Meteorological Investigations*, 21, 28–37, 1973.
- Verhoef, W. and Bach, H.: Coupled soil-leaf-canopy and atmosphere radiative transfer modeling to simulate hyperspectral multi-angular surface reflectance and TOA radiance data, *Remote Sens. Environ.*, 109, 166–182, <https://doi.org/10.1016/j.rse.2006.12.013>, 2007.
- Verhoef, W. and Bach, H.: Simulation of Sentinel-3 images by four-stream surface-atmosphere radiative transfer modeling in the optical and thermal domains, *Remote Sens. Environ.*, 120, 197–207, <https://doi.org/10.1016/j.rse.2011.10.034>, 2012.
- Vermote, E., Justice, C., Claverie, M., and Franch, B.: Preliminary analysis of the performance of the Landsat 8/OLI land surface reflectance product, *Remote Sens. Environ.*, 185, 46–56, 2016.
- Vermote, E. F., Tanré, D., Deuze, J. L., Herman, M., and Morcrette, J.-J.: Second simulation of the satellite signal in the solar spectrum, 6S: An overview, *IEEE T. Geosci. Remote*, 35, 675–686, 1997.
- Verrelst, J., Camps-Valls, G., Muñoz-Marí, J., Rivera, J. P., Veroustraete, F., Clevers, J. G., and Moreno, J.: Optical remote sensing and the retrieval of terrestrial vegetation bio-geophysical properties – A review, *ISPRS J. Photogramm.*, 108, 273–290, 2015.
- Wen, J., Liu, Q., Xiao, Q., Liu, Q., You, D., Hao, D., Wu, S., and Lin, X.: Characterizing Land Surface Anisotropic Reflectance over Rugged Terrain: A Review of Concepts and Recent Developments, *Remote Sens.-Basel*, 10, <https://doi.org/10.3390/rs10030370>, 2018.
- Widlowski, J. L., Pinty, B., Lopatka, M., Atzberger, C., Buzica, D., Chelle, M., Disney, M., Gastellu-Etchegorry, J. P., Gerboles, M., and Gobron, N.: The fourth radiation transfer model intercomparison (RAMI-IV): Proficiency testing of canopy reflectance models with ISO-13528, *J. Geophys. Res.-Atmos.*, 118, 6869–6890, 2013.
- Widlowski, J.-L., Mio, C., Disney, M., Adams, J., Andredakis, I., Atzberger, C., Brennan, J., Busetto, L., Chelle, M., and Ceccherini, G.: The fourth phase of the radiative transfer model intercomparison (RAMI) exercise: Actual canopy scenarios and conformity testing, *Remote Sens. Environ.*, 169, 418–437, <https://doi.org/10.1016/j.rse.2015.08.016>, 2015.
- Yan, K., Zhang, Y., Tong, Y., Zeng, Y., Pu, J., Gao, S., Li, L., Mu, X., Yan, G., Rautiainen, M., Knyazikhin, Y., and Myneni, R. B.: Modeling the radiation regime of a discontinuous canopy based on the stochastic radiative transport theory: Modification, evaluation and validation, *Remote Sens. Environ.*, 267, <https://doi.org/10.1016/j.rse.2021.112728>, 2021.
- Yang, B., Knyazikhin, Y., Xie, D., Zhao, H., Zhang, J., and Wu, Y.: Influence of Leaf Specular Reflection on Canopy Radiative Regime Using an Improved Version of the Stochastic Radiative Transfer Model, *Remote Sens.-Basel*, 10, 1632, <https://doi.org/10.3390/rs10101632>, 2018.
- Yin, G., Li, A., Zhao, W., Jin, H., Bian, J., and Wu, S.: Modeling Canopy Reflectance Over Sloping Terrain Based on Path Length Correction, *IEEE T. Geosci. Remote*, 55, 4597–4609, <https://doi.org/10.1109/tgrs.2017.2694483>, 2017.
- Zeng, Y., Li, J., Liu, Q., Huete, A. R., Xu, B., Yin, G., Fan, W., Ouyang, Y., Yan, K., Hao, D., and Chen, M.: A Radiative Transfer Model for Patchy Landscapes Based on Stochastic Radiative Transfer Theory, *IEEE T. Geosci. Remote*, 58, 2571–2589, <https://doi.org/10.1109/tgrs.2019.2952377>, 2020.
- Zhao, K., Popescu, S., and Nelson, R.: Lidar remote sensing of forest biomass: A scale-invariant estimation approach using airborne lasers, *Remote Sens. Environ.*, 113, 182–196, <https://doi.org/10.1016/j.rse.2008.09.009>, 2009.